THE ASTROPHYSICAL JOURNAL, 347:68–73, 1989 December 1

MAXIMUM ENTROPY DECONVOLUTION OF THE OPTICAL JET OF 3C 273

I. N. EVANS
Space Telescope Science Institute
H. C. FORD[1] AND X. HUI[1]
University of Michigan, and Space Telescope Science Institute
Received 1988 October 4; accepted 1989 June 8

ABSTRACT

We have applied the technique of maximum entropy image restoration to the problem of deconvolving the point spread function from a deep, high-quality *V* band image of the optical jet of 3C 273. The resulting maximum entropy image has an approximate spatial resolution of 0".6 and has been used to study the morphology of the optical jet. Four regularly spaced optical knots are clearly evident in the data, together with an optical "extension" at each end of the optical jet. The jet oscillates around its center of gravity, and the spatial scale of the oscillations is very similar to the spacing between the optical knots. The jet is marginally resolved in the transverse direction and has an asymmetric profile perpendicular to the jet axis. We present the distribution of *V* band flux along the length of the jet, and accurate astrometry of the optical knot positions.

Subject headings: galaxies: jets — image processing — quasars

I. INTRODUCTION

Although the jet emanating from the quasar 3C 273 has been studied now for 25 yr since the radio source was identified with its optical counterpart by Schmidt (1963), it has remained somewhat of an enigma. During the intervening period, the jet has been extensively studied in virtually every waveband from the γ-ray and X-ray bands (e.g., Bignami *et al.* 1981; Harris and Stern 1987) to the infrared and radio (e.g., Henry, Becklin, and Telesco 1984; Perley 1984). At radio wavelengths, the flux emitted by the jet increases by 2 orders of magnitude from the inner end of the jet before terminating in a radio hotspot, 3C 273A, $\sim 21''$ from the quasar (Conway, Davis, and Foley 1981). In contrast, the optical jet is largely devoid of any strong brightness gradient and terminates in an optical knot $\sim 20''$ from the quasar. Polarimetric observations in the radio regime (Perley 1984; Flatters and Conway 1985) indicate that synchrotron radiation is the source of the jet emission in that waveband. Where the jet is optically visible, the magnetic field lines run parallel to the jet axis, but there is an abrupt field reversal in the radio hotspot beyond the end of the optical jet. Recent observations by Scarrott and Warren-Smith (1987) indicate strong polarization with a similar field structure in the optical.

Recently, several imaging studies of the jet have been conducted in the optical waveband (e.g., Lelièvre *et al.* 1984; Röser and Meisenheimer 1986; Hayes and Sadun 1987), but these have been hampered by the low surface brightness of the optical jet and the effects of atmospheric seeing. Provided that the signal-to-noise ratio of the data is adequate, image restoration techniques may be applied to deconvolve the point spread function from the image to yield an improvement in spatial resolution. A technique which offers great promise for such problems is *maximum entropy*, which has been applied to astronomical image deconvolutions at γ-ray, X-ray, and radio wavelengths (e.g., Gull and Daniel 1978; Skilling, Strong, and Bennett 1979; Willingale 1981), and has also been applied to deconvolution of optical images of the jet in M87 (Bryan and Skilling 1980; Perryman 1981).

We have recently obtained a deep, high-quality *V* band image of the jet of 3C 273 and applied the maximum entropy method to the task of deconvolving the point-spread function (PSF) from the optical image. Our reasons for conducting this study are threefold. First, we wished to investigate the morphological structure of the optical jet at higher spatial resolution and data quality than previous studies in order to confirm the existence of the faint knots and features reported by Lelièvre *et al.* (1984). We also wanted to verify the reported transverse asymmetry of the jet profile and to study the quasi-periodic placement of the optical knots and the wiggles of the jet. Second, we intended to derive accurate astrometric positions for the optical knots along the jet for use in planning observations of the jet with the Faint Object Spectrograph (FOS) on board the Hubble Space Telescope (HST). Finally, we wanted to test the applicability of maximum entropy image restoration technique to high-quality CCD imaging data and demonstrate the gains obtained from its application.

II. OBSERVATIONS

The data were obtained under photometric conditions at the f/2.66 prime focus of the 3.8 m telescope at the Cerro Tololo Inter-American Observatory on the night of 1988 April 12–13, using the prime focus CCD camera with the TI #1 detector. A format of 800 × 800 pixels ($\sim 240'' \times 240''$ on the sky) was employed, together with a pixel size of 15 μm × 15 μm (0".30 × 0".30 on the sky).

A deep 900 s exposure through a *V* band filter was obtained in $\sim 1".2$ seeing. The exposure time was planned to yield a minimum signal-to-noise ratio of $\sim 30:1$ per pixel in the jet so that the image would be suitable for maximum entropy processing. The nucleus of 3C 273 was positioned $\sim 4''$ off the east edge of the frame near the NE corner of the CCD (the furthest corner from the onchip amplifier) to avoid saturation effects which would otherwise arise from direct exposure to the light from the quasar.

[1] Visiting Astronomer, Cerro Tololo Inter-American Observatory, operated by the Association of Universities for Research in Astronomy, Inc., under contract with the National Science Foundation.

The data were reduced in the following manner. First, the frame was trimmed to the active area of the detector (791 × 797 pixels), and the DC bias level and structure was corrected by subtracting the median of 25 bias frames. Second, a single bias-subtracted dark frame of equal exposure time was subtracted to correct for the dark current noise. Third, pixel-to-pixel variations in sensitivity were removed by dividing by the median of 5 V band flat field frames obtained from exposures of color-balanced quartz lamps reflected off the dome. A photometric calibration was applied to the data by comparison of the observed count rates with those obtained from the Oke (1974) spectrophotometric standard star L745−46A and also a short exposure of the quasar itself. No photometric color terms were derived or applied to the data.

III. MAXIMUM ENTROPY IMAGE DECONVOLUTION

Deconvolution of the image data was performed using the maximum entropy method. This technique determines the optimum map of the intensity distribution on the sky possessing the largest configurational entropy (or alternatively, which has the smoothest possible structure) which is consistent with the observational data.

Following the notation of Skilling and Gull (1985), for any image we can define the probability that the flux in the ijth pixel is f_{ij} by

$$p_{ij} = f_{ij} / \sum f_{ij} \,, \tag{1}$$

where the total flux in the image is $\sum f_{ij}$, and we assume that the pixels have uniform area and sensitivity. Shannon (1948) has demonstrated that this distribution of probabilities has a well-defined information content given by (minus) its *entropy*, where the latter is defined as

$$S = -\sum p_{ij} \log p_{ij} \,. \tag{2}$$

An alternate form of the entropy, $S = -\sum \log p_{ij}$, has been proposed by Burg (1967), but suffers from the problem of spontaneous line splitting (e.g., Chen and Stegen 1974; Fougere, Zawalick, and Radoski 1976), and has been shown (Gull and Skilling 1985) not to be appropriate for studying the spatial distribution of intensity over an image.

We define the *constraint function*, C, by

$$C = \sum \frac{F_{ij} - D_{ij}}{\sigma_{ij}^2} \,, \tag{3}$$

where the F_{ij} are the result of convolving the f_{ij} with the PSF, the D_{ij} are the observational data, and σ_{ij}^2 is the variance associated with the datum D_{ij}. The problem of finding the image with the least configurational information content that is consistent with the observational data is equivalent to finding the values f_{ij} which maximize S subject to the constraint $C \leq C_0$ where C_0 is some *a priori* maximum acceptable value for C. The constraint function possesses a χ^2 distribution with an expected value equal to the number of data points. Typically, a value for C_0 is chosen to obtain a given confidence level (e.g., 99%) for the statistic C. Except in the trivial case where the unconstrained maximum of S (corresponding to the flat image with all the f_{ij} equal) has $C \leq C_0$, the constrained maximum of S lies at an extremal of $S - \lambda C$ for a suitable Lagrangian multiplier λ. From this, the f_{ij} can be determined from the equation

$$\log \mathrm{DEF} - \log f_{ij} = \lambda \left(\sum f_{ij} \right) \frac{\partial C}{\partial f_{ij}} \,, \tag{4}$$

where

$$\mathrm{DEF} = \exp \left(\sum p_{ij} \log f_{ij} \right) . \tag{5}$$

The value DEF is a weighted mean of the f_{ij} that can be interpreted as the default value to which f_{ij} will tend if there are no data pertaining to the ijth pixel.

Equations (4) and (5) can be solved numerically, and we have employed the MEMSYS package to do so. The operation of this package has been described in detail by Skilling (1986) and will not be repeated here. To minimize the computation time, a 64 × 64 pixel region encompassing the optical jet was extracted from the original image. A model for the σ_{ij} was computed by summing in quadrature the Poisson noise per pixel derived from the measured number of detected photoelectrons (prior to background subtraction) and the CCD readout noise. A two-dimensional bi-cubic spline surface fit to the image excluding the jet was computed and subtracted from the image to remove the background which has a strong radial variation in the region near the quasar. The region of the image containing the jet which was excluded from the background fit was determined iteratively, and consisted of the contiguous region for which the measured intensity was at least one standard deviation above the value expected from the computed bi-cubic spline fit. An approximation to the PSF was computed by fitting an analytical profile to the five brightest unsaturated stellar images in the CCD frame, using the STARMAN package for crowded field stellar photometry (Penny 1987). The stellar profile is well fitted by an elliptical rotated Lorentzian function with major and minor FWHM of 1″327 and 1″154 and a major axis P.A. of 6°04. The maximum entropy solution was computed in two steps. First, a solution was obtained starting from a flat initial image, and a flat default image (DEF) with an intensity equal to one-half of the mean value of the positive pixels in the image. For this first solution, we decided to follow the recommendation of Weir (1987) to overfit the data initially by choosing a low value of C_0 to minimize the well known bias of the maximum entropy solution to underfit image peaks. In this step we used a value for C_0 which was equal to 85% of the value used in the next step. Second, the maximum entropy solution was computed as before, except that the output image resulting from the first step was used as the default image, after first smoothly interpolating over any features which fell below the noise. In this second step, the value for C_0 was chosen to yield a 99% confidence level that features present in the maximum entropy map have evidence for them in the original data.

We present the original background-subtracted image of the jet and the final maximum entropy solution, in Figures 1 and 2 (Plate 1), respectively. The resolution of the maximum entropy solution varies across the image depending on the instantaneous signal-to-noise ratio, but the transverse FWHM of the jet measured from the image is ∼0″6, indicating a factor of 2 improvement in resolution over the original. This compares to the 1″0 FWHM of the electronographic V band image of Lelièvre *et al.* (1984). Since the pixel size is 0″3 × 0″3 on the sky, the maximum entropy image is critically sampled, and we cannot investigate structure in the transverse direction which has a scale smaller than 0″6. Knots A, B, C, and D, and extensions 1 and 2, (where we have used the notation of Lelièvre *et al.* 1984) are clearly evident in the maximum entropy solution. In both our original and processed images, the telescope diffraction spike at P.A. 225° is clearly visible as an extension to

1989ApJ...347...68E

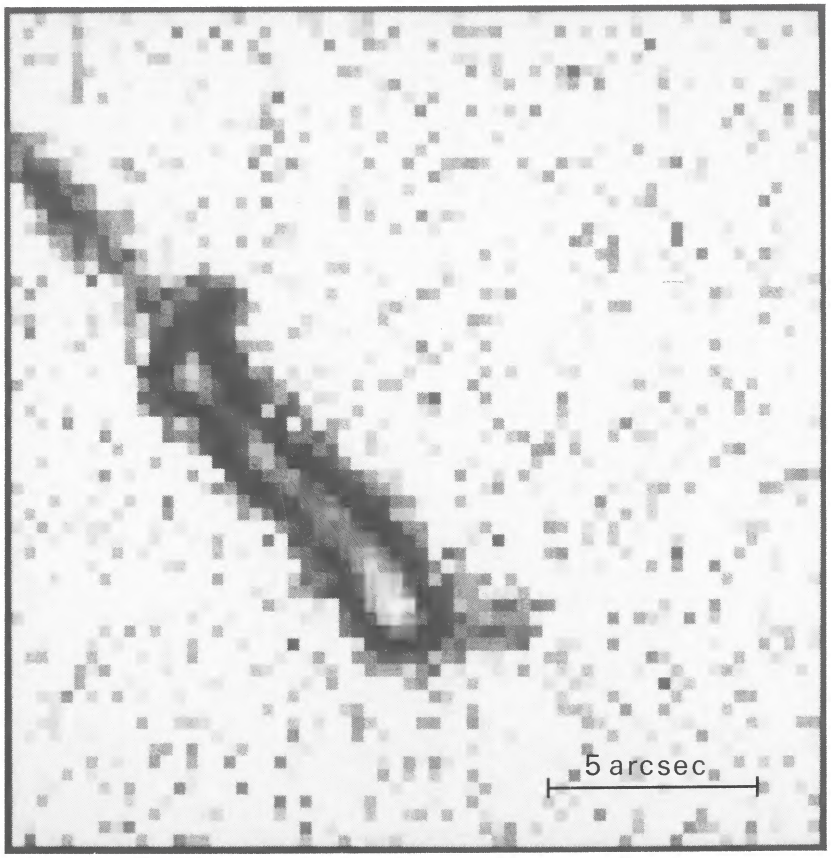

FIG. 1

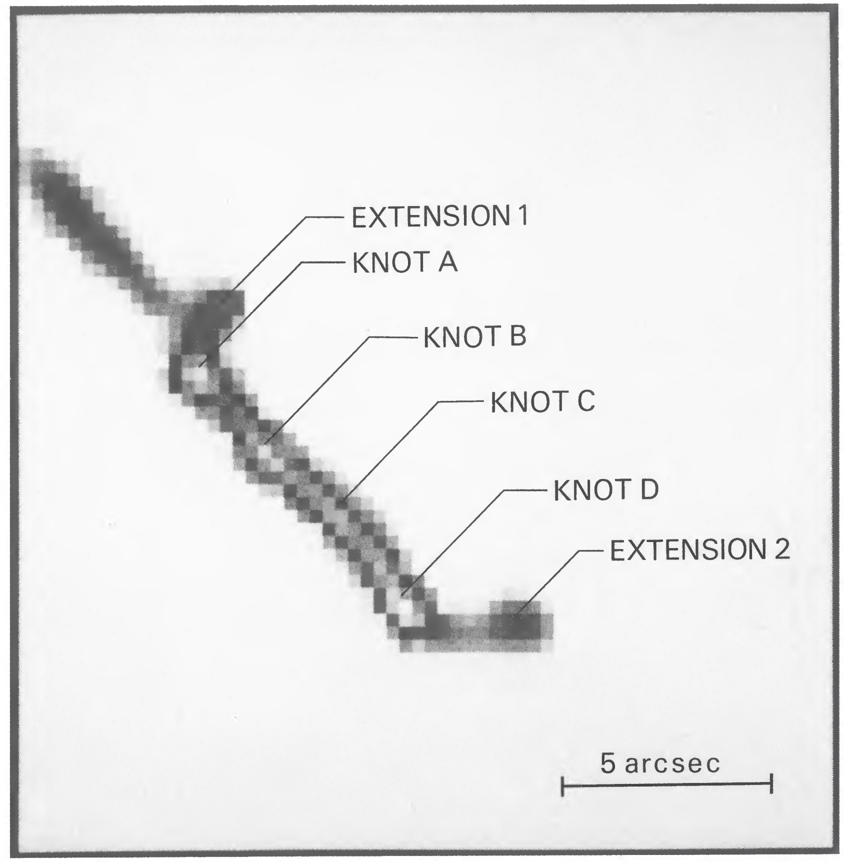

FIG. 2

FIG. 1.—Original background subtracted image of the jet. The quasar is located off the frame to the upper left. Detail of the outer regions of the frame fainter than $V = 23$ mag (arcsec)$^{-2}$ is displayed as a negative image superposed on a positive image showing detail brighter than $V = 23$ mag (arcsec)$^{-2}$. The intensity scale on either side of the break point is logarithmic, although the peak intensity of the positive image has been reproduced as white, independent of its actual surface brightness, in order to maximize the visibility of the bright features in the jet.

FIG. 2.—Same as Fig. 1, except that the maximum entropy reconstruction is shown. Knots A–D and extensions 1 and 2 are indicated.

EVANS, FORD, and HUI (*see* **347**, 69)

the northeast of the jet, making it impossible for us to confirm the apparent inner extension ("extension 3") of the jet seen in the *V* band image of Lelièvre *et al.* (1984).

To resolve the problem of critically sampling the image plane, the original image and PSF were resampled onto a finer grid. This was achieved by subdividing each pixel into a 4 × 4 array of subpixels, and then summing together the 16 frames constructed by offsetting the original image and PSF by 0, 1, 2, and 3 subpixels in the *X*-direction for each of 0, 1, 2, and 3 subpixel offsets in the *Y*-direction. A maximum entropy solution was then computed for the resampled image in the same way as before. It is essential to realize that this procedure *cannot* increase the resolution of the maximum entropy solution since no new information or additional constraints are added. However, the procedure produces a much smoother looking processed image which simplifies the morphological studies. The maximum entropy solution for the resampled image is presented in Figures 3 (Plate 2) and 4, and these images define much more clearly the locations of the four knots in the jet, as well as the structure of the extensions at either end of the jet and the wiggles in the jet itself.

IV. ASTROMETRY

Reduction of the image to an astrometric frame was conducted using the Hubble Space Telescope Guide Star Catalog (GSC1) as the primary reference. Since the GSC1 is only complete to $m_J \approx 15.5$ it was not possible to directly calibrate the CCD frame using positions from the catalog. Instead, a secondary astrometric reference frame was established by using GSC1 positions of bright stars to calibrate a 15ʹ.8 × 5ʹ.3 PDS scan of a deep red (IIIa-F plus OG570) 4 m plate of the region surrounding the quasar. The CCD frame was then astrometrically calibrated using positions derived from the 4 m plate as the secondary reference.

The centroid positions of knots A, B, C, and D, together with the centroid position of the peak visible in extension 2, were measured from the substepped maximum entropy solution,

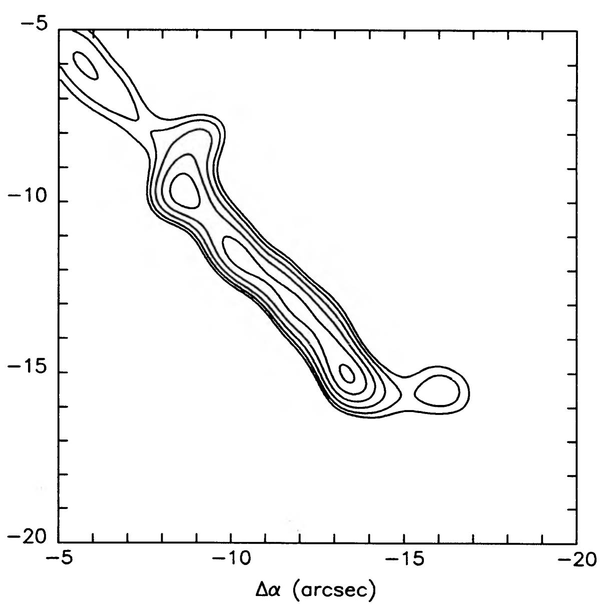

FIG. 4.—Contour plot of Fig. 3. The faintest contour indicates a flux level of $V = 26$ mag (arcsec)$^{-2}$, with successive contours each being 1 mag (arcsec)$^{-2}$ brighter. Relative displacements in α and δ (J2000.0) from 3C 273 are marked.

TABLE 1

ASTROMETRIC POSITIONS (J2000.0)

Identification	α^a	δ^a
Knot A	12ʰ29ᵐ06ˢ.12	+02°02ʹ58ʺ.3
Knot B	12 29 06.02	+02 02 56.4
Knot C	12 29 05.91	+02 02 54.8
Knot D	12 29 05.82	+02 02 52.9
Extension 2	12 29 05.64	+02 02 52.4

[a] GSC1 reference frame.

and in Table 1 we present their astrometric positions in the GSC1 reference frame. In the same reference frame, the position of 3C 273 is $\alpha = 12^h29^m06^s.71$, $\delta = +02°03ʹ07ʺ.9$ (J2000.0). Relative to the quasar, the astrometry has a formal accuracy of 0ʺ.2. The absolute position we derive for knot D is in excellent agreement (0ʺ.15) with the position measured from Figure 4 of Röser and Meisenheimer (1986), although not with the radial distance from the quasar that those authors quote in their text. Neither our position for knot D, nor the position measured from Figure 4 of Röser and Meisenheimer (1986), agree with the position of the knot reported by Scarrott and Warren-Smith (1987), and we conclude that the latter is in error.

V. DISCUSSION

Comparison of the maximum entropy images with the earlier work of Lelièvre *et al.* (1984) clearly demonstrates the improvements that are possible using this technique. The enhanced spatial resolution and signal-to-noise ratio of the reconstruction clearly confirms the existence of knot C and extensions 1 and 2, which were either difficult to see or ill-defined in the earlier work. (As mentioned previously, we cannot confirm the existence of extension 3, which was only present in the *V* band image of Lelièvre *et al.* [1984], because of the presence of the telescope diffraction spike from the quasar at almost the same position angle as the jet.) The correspondence of the features (knots A–D and extensions 1 and 2) between the images of Lelièvre *et al.* (1984) and the maximum entropy solution gives us confidence that the latter is not introducing spurious features into the reconstruction.

The jet morphology is most evident from Figures 3 and 4. The two brightest knots (A and D) delimit the ends of the optical jet and merge into extensions 1 and 2, respectively. The former appears to be a smooth continuation of the optical jet and may for example represent an oblique shock associated with the transition of the jet from a regime of highly efficient laminar flow to one of turbulent flow at the location where the optical jet becomes visible. Extension 2, on the other hand, forms a faint but clearly distinct knot with a FWHM of ∼0ʺ.8 and may be spatially resolved. From these data alone it is not possible to decide whether the extensions are directly connected with the jet or whether they are merely background objects. Neither extension is visible at radio wavelengths (Röser and Meisenheimer 1986), but extension 1 *is* visible on the *U* band image of Lelièvre *et al.* (1984) strongly suggesting that it, at least, is not a background galaxy.

At the resolution presented here, the optical jet very clearly shows evidence for wiggles. The "center of gravity" of the transverse jet profile oscillates around the mean position angle of the jet. This is shown in Figure 5, where we have taken the position angle of the jet to be 222°.0, computed as the mean P. A. between the quasar and each of the four optical knots A–D. Similar structure is observed in the arcsecond resolution

1989ApJ...347...68E

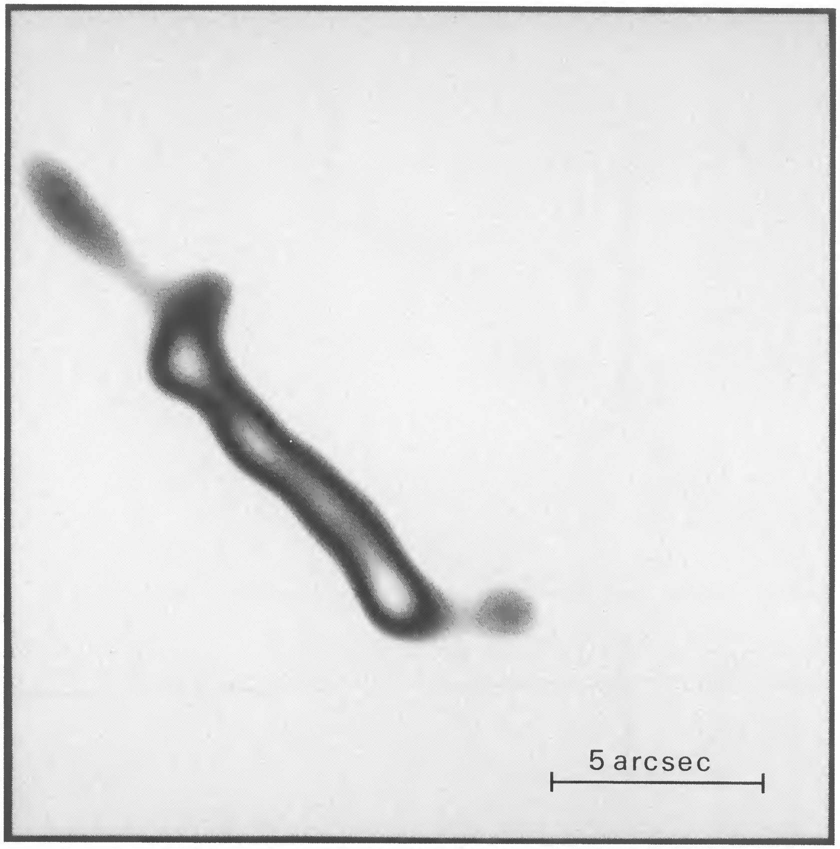

FIG. 3.—Same as Fig. 1, except that the maximum entropy reconstruction from the subsampled data is shown

EVANS, FORD, and HUI (*see* **347**, 70)

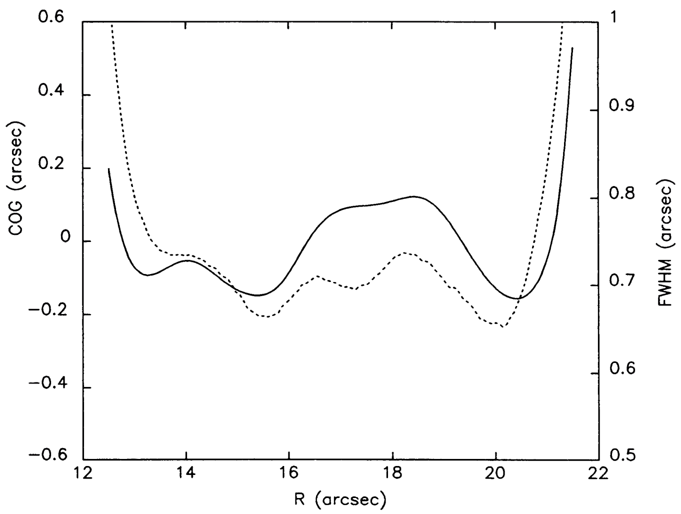

FIG. 5.—Offset of the center of gravity (*solid line*) and FWHM (*dotted line*) of the jet profile transverse to a P.A. of 222°.0 from the quasar is shown as a function of linear displacement along the jet. Extensions 1 and 2 contribute for $R \lesssim 13''$ and $R \gtrsim 20''$, respectively.

radio maps of the jet obtained at a number of wavelengths (e.g., Conway and Stannard 1975; Conway, Davis, and Foley 1981; Perley 1984). Such oscillations may be caused by several different phenomena, including the growth of helical Kelvin-Helmholtz instabilities at the boundary of a confined jet (e.g., Ferrari, Trussoni, and Zaninetti 1978), or alternatively precession of the primary collimator of the jet near its source (e.g., Rees 1978). Inspection of the figure indicates that the jet does not change direction only at the locations of the optical knots, but rather bends continuously along its length. This is particularly evident between knots C and D and implies that models which invoke deflection of an (otherwise ballistic) jet by interactions with the intergalactic medium (IGM) at the locations of the optical knots as the sole mechanism for shaping the jet cannot be correct.

The quasi-periodic nature nature of the optical structure in the jet has been previously remarked on by Lelièvre *et al.* (1984), who noted that the optical knots are regularly spaced along the jet. In fact, the knot spacing is not precisely periodic, but varies from a minimum of 2″.26 between knots B and C to a maximum of 2″.46 between knots A and B, with a mean value of 2″.37 ± 0″.10. Interestingly, the radial positions of the optical knots along the jet coincide to within 0″.2 with the greatest southerly excursions of the center of gravity of the optical jet as it oscillates around the mean jet position angle. The spatial scale length of the jet oscillations is 2″.32 ± 0″.54, which is in good agreement with that derived from the locations of the optical knots. With the exception of the region around knot C, the amplitude of the oscillations in the optical jet increases from ∼0″.04 near knot A to a maximum of ∼0″.28 near knot D. This contrasts with the data of Davis, Muxlow, and Conway (1985) who found that the amplitude of the oscillations of the radio ridge line is approximately constant, ∼0″.5 peak to peak, but that the semiwavelength of the pattern decreased systematically from ∼6″ at the core to ∼1″ at the end of the radio jet. Such data are readily interpreted in terms of a model with a precessing relativistic jet, together with deceleration of the flow along the jet due to interactions with the IGM. However, as pointed out by Conway, Davis, and Foley (1981), a precessing jet should also exhibit oscillations in brightness associated with the spatial oscillations. The radio data show no evidence for this, however, leading those authors to suggest that hydrodynamic instabilities were the most probable cause for the wiggles in the jet.

It is important for us to establish whether or not the optical jet is resolved in the transverse direction, since both Lelièvre *et al.* (1984) and also Scarrott and Warren-Smith (1987) suggest that the jet profile is not symmetric in the transverse direction. Also in Figure 5 we present a plot of the FWHM of the jet transverse to a P.A. of 222°. Inspection of the figure indicates that the measured transverse FWHM of the jet varies with radial position along the jet from a minimum value of 0″.65 near knot D to a maximum value of 0″.74 between knots C and D (we have excluded from consideration the regions near both ends of the jet where there are contributions to the measured jet FWHM from extensions 1 and 2). However, the spatial resolution of the maximum entropy reconstruction is not constant across the image, but depends on the instantaneous signal-to-noise ratio at each point in the image. Those areas of the image which have the highest signal-to-noise ratio also have the highest spatial resolution. We can see from the figure that this effect may be evident in the data, since the region of the jet near knot D which has the lowest transverse FWHM is also the region with the highest signal-to-noise ratio. On the other hand, the region between knots C and D shows the largest transverse FWHM, but does not have the lowest signal-to-noise ratio in the jet (which occurs between knots A and B). Indeed, the variation of the signal-to-noise ratio along the jet is actually quite small (∼5%), and we would not expect that the spatial resolution should change dramatically along the jet. Consideration of these points leads us to believe that the observed variation of the transverse FWHM of the jet is largely real, implying that the jet is marginally resolved in the transverse direction.

In addition to the direct measurements of the jet FWHM presented above, we have also observed the transverse asymmetry of the jet detected previously. We have chosen to parameterize this asymmetry in terms of the asymmetry function proposed by Whittle (1985) for measuring the asymmetry of emission line profiles. If we make a transverse cut across the jet profile and measure the distances a and b between the profile median and the positions on the profile to the SE and NW beyond which is 10% (in each direction) of the total flux in the profile, then we define the value of the asymmetry function at the 20% flux level to be $A(20\%) = (a - b)/(a + b)$. The value of the asymmetry function at different flux levels is computed in an analogous manner. Defined in this fashion, the asymmetry function of a symmetric profile would be zero, while a negative asymmetry function would indicate a transverse gradient stronger to the SE than to the NW. In Figure 6 we present the values of the asymmetry function at the 20%, 50%, and 80% flux levels as a function of position along the jet. Inspection of the figure clearly shows the presence of the asymmetry in the transverse jet profile at low flux levels, with the jet profile becoming more symmetric as the flux level is increased. For a given flux level, the transverse jet profile is most symmetric at the locations of the optical knots, with increased asymmetry between the knots. The greatest asymmetry occurs in the regions where the jet flux is lowest. This suggests that the asymmetry is associated with the underlying flow pattern and may be independent of the physical processes, such as shocks, turbulence, and pinch instabilities (e.g., Chan and Henriksen

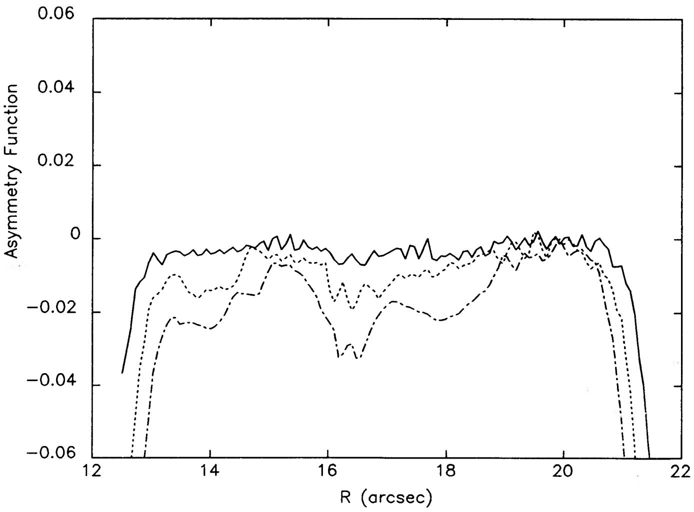

FIG. 6.—Asymmetry functions $A(80\%)$ (*solid line*), $A(50\%)$ (*dotted line*), and $A(20\%)$ (*dash-dotted line*), as a function of linear displacement along the jet. Extensions 1 and 2 contribute for $R \lesssim 13''$ and $R \gtrsim 20''$, respectively. The asymmetry function is defined in the text.

1980; Blandford and Königl 1982), responsible for forming the optical knots.

Since our observations were conducted through a broad-band filter, we must now consider the contribution of differential atmospheric refraction to the measured width of the jet, and whether the transverse asymmetry of the optical jet can be explained through this mechanism. During the exposure, a source which emitted uniformly throughout the V band would be differentially refracted by 0$''$.32 over the effective width of the band. The mean parallactic angle during the exposure was 27°, so that the contribution in the direction transverse to the jet would be $\sim$0$''$.08. This is of the order of the variation of the observed jet FWHM. Because of the red color of the jet (e.g., Röser and Meisenheimer 1986; Hayes and Sadun 1987), differential refraction will yield an asymmetric transverse jet profile with a steeper gradient on the southern (red) side of the jet than on the northern (blue) side. Assuming that the mean optical jet fluxes of Röser and Meisenheimer (1986) in the blue and red bands can be smoothly interpolated across the V band, differential refraction would contribute $\sim$0$''$.06 to the transverse width of the optical jet. Although of similar magnitude, we do not believe that this effect can account for the observed transverse asymmetry of the jet, since the asymmetry is also evident in the data of Lelièvre *et al.* (1984) and Scarrott and Warren-Smith (1987). Since the data obtained by both these authors comes from telescopes located in the northern hemisphere (CFHT and the INT, respectively), any transverse asymmetry which is due to differential refraction should appear on the *opposite* side of the jet from our own observations, which were obtained in the southern hemisphere.

The radial distributions of the V band flux along the optical jet derived from both the original background subtracted image and the maximum entropy solution are shown in Figure 7. In both cases the data are integrated across the total width of the jet in the transverse direction and presented in units of magnitudes per arcsec of jet length. The distribution of V band flux along the jet is similar to that seen in the blue and red data of Röser and Meisenheimer (1986), and also the unfiltered broad-band ($\sim$4500–10000 Å) data of Scarrot and Warren-Smith (1987), with the exception of the inner end of the jet where extension 1 contributes to the fluxes presented here. The strong contributions of the optical knots to the overall jet flux is clearly visible in the maximum entropy solution in Figure 7, and the flux from the underlying jet component (i.e., excluding the contributions of the knots) appears to be steadily increasing toward the outer end of the optical jet.

VI. CONCLUSIONS

We have applied the maximum entropy method to deconvolve the point spread function from a deep optical V band image of the jet of 3C 273. The reconstructed image of the jet has a high signal-to-noise ratio and a spatial resolution of $\sim$0$''$.6. Comparison of the maximum entropy solution with the lower resolution V band image of Lelièvre *et al.* (1984) demonstrates that this technique can be very successfully applied to high-quality CCD imaging data, yielding a factor of 2 gain in spatial resolution. The features marginally detected in both the data of Lelièvre *et al.* (1984) and our original image are clearly evident in the maximum entropy reconstruction. We do not see any evidence to suggest that spurious features have been introduced into the reconstructed image.

Accurate astrometric positions for the optical knots in the jet were measured from the reconstructed image, using the Hubble Space Telescope Guide Star Catalog as the primary reference frame. These positions have an formal accuracy of 0$''$.2 relative to the quasar and will be used by the Faint Object Spectrograph Investigation Definition Team to plan Gauranteed Time Observations of the optical jet with the FOS aboard the HST.

The morphology of the optical jet is clearly visible from the maximum entropy reconstruction. There are four optical knots spaced evenly along the length of the jet, together with two additional features, or "extensions," at either end of the jet. The center of gravity of the optical jet oscillates smoothly around its mean position angle, with a spatial scale length nearly identical to the knot spacing. In the direction transverse to the jet, both the FWHM and the asymmetry of the jet profile vary with position along the jet, suggesting that the jet is resolved at the spatial resolution of the maximum entropy

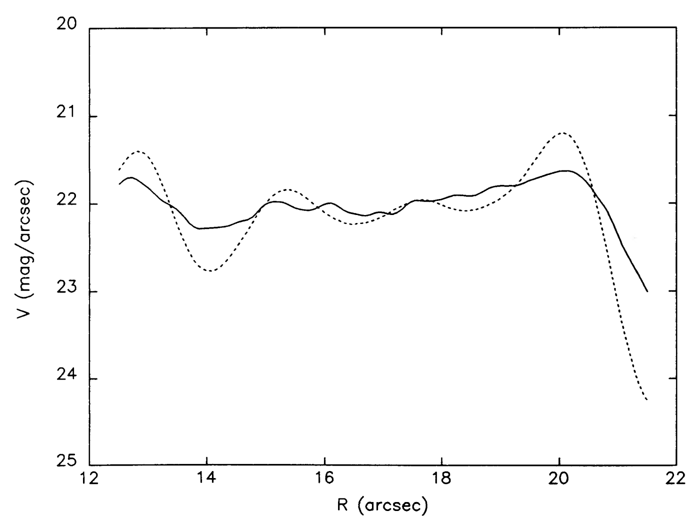

FIG. 7.—The radial distribution of the V band flux in the original background subtracted image (*solid line*) and the maximum entropy reconstruction of the subsampled data (*dotted line*) as a function of linear displacement along the jet. The flux is integrated over the total width of the jet.

image. The asymmetry of the transverse profile is most evident at lower flux levels, and is in the same sense as previously observed (Lelièvre *et al.* 1984; Scarrott and Warren-Smith 1987), although there may be some contribution from differential atmospheric refraction in our data. Finally, we have measured the distribution of V band optical flux along the jet and find it to be in good agreement with the distributions of blue and red flux observed by Röser and Meisenheimer (1986).

The authors would like to thank John Skilling for many stimulating discussions on maximum entropy and Bayesian methods, and for generously making his maximum entropy system (MEMSYS) available to us for this work. Additional discussions and many valuable suggestions regarding maximum entropy processing were made by Keith Horne. Peter Wehinger and Susan Wyckoff kindly allowed us to use PDS scans (made by Carla Landenburger) of a deep 3.6 m photographic plate for the astrometric calibration. The latter was carried out by the Guide Star Operations group here at the Space Telescope Science Institute, especially Brian McLean and Caroline Simpson, plus useful discussions with Barry Lasker and Mario Lattanzi. Finally, the referee, Nigel Sharp, made several valuable suggestions which have helped to clarify the presentation of the results of this paper significantly. This work was supported in part through National Aeronautics and Space Administration contract NAS 5-29293.

REFERENCES

Bignami, G. F., *et al.* 1981, *Astr. Ap.*, **93**, 71.
Blandford, R. D., and Königl, A. 1982, *Ap. Letters Comm.*, **20**, 15.
Bryan, R. K., and Skilling, J. 1980, *M.N.R.A.S.*, **191**, 69.
Burg, J. P. 1967, paper presented at the 37th meeting of the Society of Exploration Geophysicists (Oklahoma City).
Chan, K. L., and Henriksen, R. N. 1980, *Ap. J.*, **241**, 534.
Chen, W. Y., and Stegen, G. R. 1974, *J. Geophys. Res.*, **79**, 3019.
Conway, R. G., Davis, R. J., and Foley, A. R. 1981, *Nature*, **294**, 540.
Conway, R. G., and Stannard, D. 1975, *Nature*, **255**, 310.
Davis, R. J., Muxlow, T. W. B., and Conway, R. G. 1985, *Nature*, **318**, 343.
Ferrari, A., Trussoni, E., and Zaninetti, L. 1978, *Astr. Ap.*, **64**, 433.
Flatters, C., and Conway, R. G. 1985, *Nature*, **314**, 425.
Fougere, P. F., Zawalick, E. J., and Radoski, H. R. 1976, *Phys. Earth Planet. Inter.*, **12**, 201.
Gull, S. F., and Daniell, G. J. 1978, *Nature*, **272**, 686.
Gull, S. F., and Skilling, J. 1985, in *Maximum-Entropy and Bayesian Methods in Inverse Problems*, ed. C. R. Smith, and W. T. Grandy, Jr. (Dordrecht: Reidel), p. 287.
Harris, D. E., and Stern, C. P. 1987, *Ap. J.*, **313**, 136.
Hayes, J. J. E., and Sadun, A. C. 1987, *A.J.*, **94**, 871.
Henry, J. P., Becklin, E. E., and Telesco, C. M. 1984, *Ap. J.*, **280**, 98.
Lelièvre, G., Nieto, J.-L., Horville, D., Renard, L., and Servan, B. 1984, *Astr. Ap.*, **138**, 49.
Oke, J. B. 1974, *Ap. J. Suppl.*, **27**, 21.
Penny, A. J. 1987, *STARMAN Version 0.9: A User's Guide* (Baltimore: Space Telescope Science Institute).
Perley, R. A. 1984, in *IAU Symposium 110, VLBI and Compact Radio Sources*, ed. R. Fanti, K. Kellermann, and G. Setti (Dordrecht: Reidel), p. 153.
Perryman, M. A. C. 1981, in *Proc. 2d ESO/ESA Workshop on the Space Telescope and Co-ordinated Ground Based Research* (Paris: European Space Agency), p. 25.
Rees, M. J. 1978, *Nature*, **275**, 516.
Röser, H.-J., and Meisenheimer, K. 1986, *Astr. Ap.*, **154**, 15.
Scarrott, S. M., and Warren-Smith, R. F. 1987, *M.N.R.A.S.*, **228**, 35P.
Schmidt, M. 1963, *Nature*, **197**, 1040.
Shannon, C. E. 1948, *Bell System Tech. J.*, **27**, 379.
Shore, J. E., and Johnson, R. W. 1980, *IEEE Trans. Inf. Theory*, **IT-26**, 26.
Skilling, J. 1986, in *Maximum Entropy and Bayesian Methods in Applied Statistics*, ed. J. H. Justice (Cambridge: Cambridge University Press), p. 179.
Skilling, J., and Gull, S. F. 1985, in *Maximum-Entropy and Bayesian Methods in Inverse Problems*, ed. C. R. Smith and W. T. Grandy, Jr. (Dordrecht: Reidel), p. 83.
Skilling, J., Strong, A. W., and Bennett, K. 1979, *M.N.R.A.S.*, **187**, 145.
Weir, N. 1987, B.A. thesis, Harvard College.
Whittle, M. 1985, *M.N.R.A.S.*, **213**, 1.
Willingale, R. 1981, *M.N.R.A.S.*, **194**, 359.

IAN N. EVANS, HOLLAND C. FORD, and XIAOHUI HUI: Space Telescope Science Institute, 3700 San Martin Drive, Baltimore, MD 21218

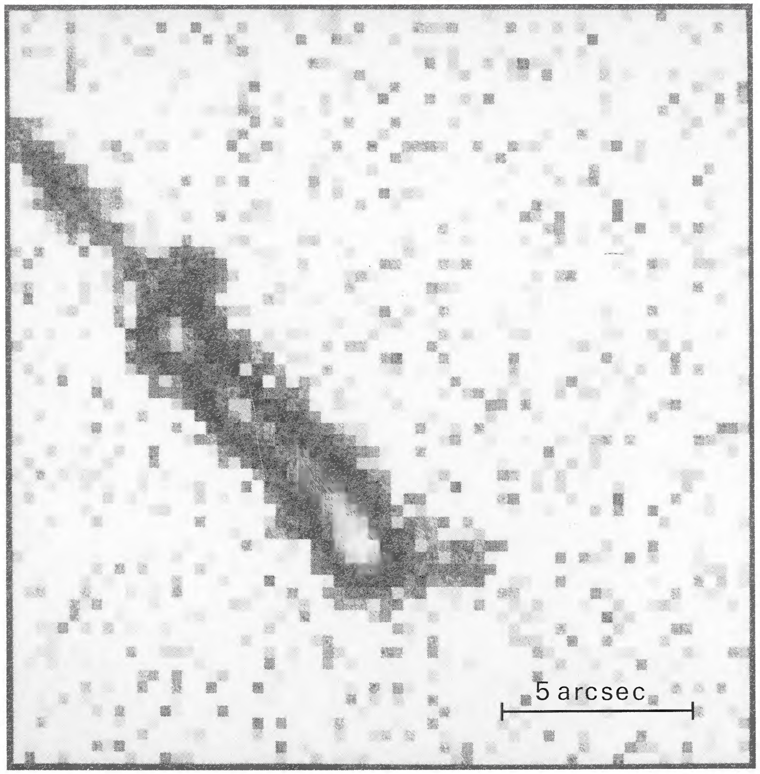

Fig. 1

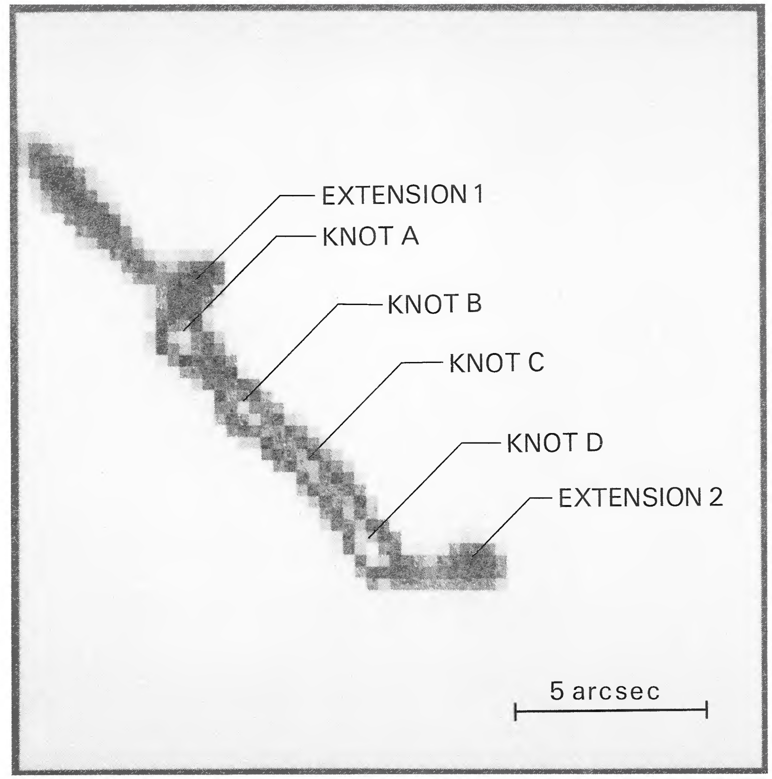

Fig. 2

Fig. 1.—Original background subtracted image of the jet. The quasar is located off the frame to the upper left. Detail of the outer regions of the frame fainter than $V = 23$ mag (arcsec)$^{-2}$ is displayed as a negative image superposed on a positive image showing detail brighter than $V = 23$ mag (arcsec)$^{-2}$. The intensity scale on either side of the break point is logarithmic, although the peak intensity of the positive image has been reproduced as white, independent of its actual surface brightness, in order to maximize the visibility of the bright features in the jet.

Fig. 2.—Same as Fig. 1, except that the maximum entropy reconstruction is shown. Knots A–D and extensions 1 and 2 are indicated.

Evans, Ford, and Hui (*see* **347**, 69)